Lab on a Chip

PAPER

View Article Online
View Journal | View Issue

Cite this: *Lab Chip*, 2024, **24**, 5398

A multimodal digital microfluidic testing platform for antibody-producing cell lines†

Jeremy T. Lant, [ab] Jurgen Frasheri,[bc] Taehong Kwon,[d] Camille M. N. Tsang,[b] Bingyu B. Li,[bc] Sheldon Decombe,[ab] Alexandros A. Sklavounos, [ab] Samin Akbari[d] and Aaron R. Wheeler *[abc]

Received 27th September 2024,
Accepted 11th November 2024

DOI: 10.1039/d4lc00816b

rsc.li/loc

In recent years, monoclonal antibodies (mAbs) have become a powerful tool in the treatment of human diseases. Currently, over 100 mAbs have received approval for therapeutic use in the US, with wide-ranging applications from cancer to infectious diseases. The predominant method of producing antibodies for therapeutics involves expression in mammalian cell lines. In the mAb production process, significant optimization is typically done to maximize antibody titres from cells grown in bioreactors. Therefore, systems that can miniaturize and automate cell line testing (*e.g.*, viability and antibody production assays) are valuable in reducing therapeutic mAb development costs. Here we present a novel platform for cell line optimization for mAb production using digital microfluidics. The platform enables testing of cell culture samples in 6–8 μL droplets with semi-automated viability, media pH, and antibody production assays. This system provides a unique bridge between cell growth and productivity metrics, while minimizing culture volume requirements for daily testing. We propose that this technology and its future iterations has the potential to help reduce the time-to-market and development costs of antibody-producing cell lines.

Introduction

In 1986, the first monoclonal antibody (mAb) was approved for therapeutic use by the United States Food and Drug Administration (US FDA).[1,2] Today, over 100 therapeutic mAbs have US FDA approval,[3] representing a market size of over $100 billion USD.[4] While bacteria and eukaryotic micro-organisms (*e.g.* yeast) are generally the most cost-effective hosts for recombinant protein production,[5] the majority of therapeutic mAbs are produced in mammalian cells.[3] Mammalian cells are capable of reproducing the folding, post-translational modification, and secretion behaviours of natural human antibodies.[5] Proper folding and post-translational modification are essential for antibodies that are safe and effective for use in humans.[5,6] Preferred mammalian cell lines can be grown in media free of animal by-products,[7,8] and benefit from a wide variety of available genetic tools for engineering cell lines.[9] Since the first US FDA-approved mAb was produced in 1985,[1] antibody yields have improved substantially from ~50 mg L^{-1} to, in some reports, over 10 g L^{-1} culture.[9] However, therapeutic monoclonal antibodies remain one of the most expensive classes of drug on the market, with average yearly treatment costs often exceeding $100 000 USD per patient.[10]

A major factor in the cost of therapeutic mAbs is the need to test large libraries of recombinant cell lines in the development process. When a new therapeutic mAb candidate is identified, DNA sequences encoding the mAb are typically introduced into the genome of cells. In many cases, genomic integration is random, and integration sites can greatly influence mAb expression levels.[11,12] For this reason, high-yield clones are isolated from polyclonal cell populations and expanded from a single cell.[13] This process can take from four to over twenty weeks depending on the method of cell isolation and expansion.[13] In addition, numerous other design features such as codon optimization, promoter sequences, signal peptides, balancing of heavy/light chain expression, and more can be optimized for maximal expression of the mAb.[9]

Changes to an antibody sequence or means of expressing it can influence the optimal growth conditions for a cell line. Indeed, optimal media feeding paradigms, associated with metabolic rates and pH stability of the media, differ greatly between cell lines.[14–16] Preferably, media formulations and

[a] *Department of Chemistry, University of Toronto, Toronto, Ontario, Canada. E-mail: aaron.wheeler@utoronto.ca*
[b] *Donnelly Centre for Cellular and Biomolecular Research, University of Toronto, Toronto, Ontario, Canada*
[c] *Institute of Biomedical Engineering, University of Toronto, Toronto, Ontario, Canada*
[d] *Sartorius Stedim North America Inc., Marlborough, MA, USA*
† Electronic supplementary information (ESI) available. See DOI: https://doi.org/10.1039/d4lc00816b

feeding paradigms should be tested early in the cell line expansion process, to minimize the timeline and resource costs per cell line. Valuable parameters in assessing cell line performance include cell viability, antibody production titre, and measures of cell metabolism or media consumption, including media pH. Interestingly, some studies have shown that dynamically modifying media pH in antibody-producing cell cultures can increase yields substantially.[15,17] Hence, testing culturing strategies early in the cell line development process is critical to assess potential productivity in large-scale culture. However, given that early-stage testing occurs during the expansion process from single cells, platforms that utilize smaller volumes of culture sample are preferred, to avoid extending the expansion timeline.

Several platforms have been developed for testing cell line growth characteristics in small volumes, and other platforms have been developed for testing mAb productivity from larger scale cultures. Commercially available platforms such as the S.NEST™ (CYTENA), BioLector XT (Beckman Coulter), or Ambr® 15 (Sartorius) enable small scale testing of media formulations, feeding paradigms, or gas perfusion conditions in volumes of 100 μL to 15 mL. Automated microfluidic platforms have also been demonstrated for in-line[18–20] or off-line[21] testing of mAb productivity from mammalian cell bioreactors. However, there is an unmet need for automated, microscale platforms that can simultaneously test for parameters associated with both cell growth and mAb productivity.

Here, we present a novel platform for testing mAb-producing mammalian cell lines using digital microfluidics (DMF). Digital microfluidic devices use patterned arrays of electrodes to translocate droplets in devices lacking standard, enclosed 'microchannel' structures. We and others have demonstrated the use of digital microfluidics to automate and miniaturize a wide range of experimental protocols, including mammalian cell culture[22–25] and enzyme-linked immunosorbent assays (ELISA).[26–28] Importantly, extensive studies in the past have demonstrated that the electrostatic forces used in DMF droplet movement are not toxic to cells,[29] making DMF an attractive platform for automating cell culture experiments. In this work, we present a novel DMF design capable of performing assays relevant to the development of therapeutic mAb producing cell lines. The device can mix and dispense droplets with high precision as well as test for cell viability, antibody titer, and media pH, all from a single sample of less than ten microliters. The new system features several technological innovations relative to the state of the art, including the first reports of 'solid-state optical pH sensing on DMF', 'immunoassay plus pH sensing on DMF', and 'combined cell viability, antibody titer, and pH sensing in a sub-100 μL volume'. More importantly, the system addresses a critical need – automated, miniaturized mammalian cell culture analysis – that could be useful for a wide range of applications in biologic drug discovery and optimization.

Materials and methods

DMF device fabrication

DMF devices were fabricated in the University of Toronto/National Research Council Centre for Research and Applications in Fluidic Technologies (CRAFT). Chromium-glass substrates coated with AZ 1500 photoresist were purchased from Telic company (Valencia, CA, USA). Custom photomasks were designed in AutoCAD 2023 and mask writing was done using a Heidelberg μPG 501 Mask Maker. Photolithography and wet etching procedures were completed as previously described.[30] Parylene-C and fluoropel layers were deposited as previously described.[30]

The electrode design on the bottom plate (chromium-on-glass) consisted of a modular ~20 × 18 mm arrangement of 19 electrodes (referred to as the "Cellspot" design). Each 19-electrode feature was designed to intercalate with another feature on the opposite side of the device, and 6 features were accommodated on each 76.2 × 76.2 × 1.0 mm chromium-glass substrate. Thirty-five micrometer gaps were designed between electrodes and adjacent electrodes were intercalated using either protruding corners or a fine interdigitation design consisting of 210 μm spaced wave lines, similarly to previously described designs.[31]

The 19-electrode Cellspot design consists of electrode arrangements designated for mixing, dispensing, and loading samples onto adhered analytical sensing patches. Briefly, a circular mixing region (with diameter 8 mm) comprises four quarter-pie-shaped electrodes surrounding an imaging window (w_i, with diameter 2 mm). A dispensing region, indented roughly 1 mm into one of the quarter-pie-shaped electrodes in the mixing region, comprises a linear array of two roughly rectangular electrodes (2.4 × 3.2 mm) and a circular "test-droplet electrode" (diameter 2 mm). An FLISA region comprises nine roughly square electrodes (2 mm × 2 mm), positioned adjacent to the dispense region, with a cut-out for the test-droplet electrode. Finally, a load region comprises a single roughly rectangular electrode (5.2 × 8.2 mm) adjacent to one of the quarter-pie electrodes in the mixing region (where the quarter-pie electrode features two roughly square 1 × 1 mm fingers penetrating into the load electrode), and a pH region comprises two electrodes and a large transparent circular pH window (w_p, with diameter 2.3 mm) that together occupy a roughly rectangular footprint (7.4 × 5.9 mm) that is recessed roughly 0.6 mm into one of the quarter-pie shaped electrodes. All electrodes were independently wired with 0.1 mm-wide chromium traces spaced at least 0.1 mm apart. Traces were connected to square contacts that interface with the pogo-pin array on a Dropbot system (Sci-Bots Inc.; Toronto, ON, Canada).

Digital microfluidic top plates consisted of 25 mm × 75 mm × 0.7 mm ITO coated glass (Riley Supplies; Richmond Hill, BC, Canada) coated with 1% FluoroPel as previously described.[30] Digital microfluidic devices were assembled by securing a top plate to a bottom plate with 202 μm thick double coated, double sided tape acrylic adhesive (3M; GPT-

020F; Saint Paul, MN, USA), with or without first integrating a pH sensor patch (described below).

Devices were controlled by using the open-source DropBot system[32] (version 3.0, https://github.com/sci-bots/dropbot-v3). A custom file was designed in AutoCAD 2023 to control the novel device design using MicroDrop software (version 2.31.1, https://github.com/sci-bots/microdrop). The design consisted of two layers: a "device" layer with simplified versions of the bottom-plate DMF design shapes and removed wires, and a "connections" layer with lines drawn connecting the shapes in the device layer. The AutoCAD .dxf file was converted to a .svg file in Inkscape and imported into the MicroDrop 3.0 software. Electrode channel numbers corresponding to the pogo pin index numbers used in the DropBot instrument were assigned within the MicroDrop 3.0 software.

Magnetic plate fabrication

Rectangular 6 × 3 mm holes were cut in a 0.7 mm thick, polyethylene terephthalate glycol (PETG) plate using a Full Spectrum Laser Cutter. Rectangular 6 × 3 × 0.7 mm neodymium magnets were inserted in the holes and secured with tape. The outer perimeter of the magnetic plate was cut to fit in a DropBot instrument in place of the spacer, which lifts devices to contact with the instrument.

Cell culture

A Chinese Hamster Ovary (CHO) DG44 cell line engineered by Sartorius Stedim Cellca GmbH (Goettingen, Germany) was used for all cell-based experiments. The cell line expresses Adalimumab biosimilar, a human immunoglobulin G (IgG) antibody that has been integrated into the CHO cell genome. Cells were maintained in a proprietary medium supplemented with 15 nM methotrexate (Fisher BioReagents, Pittsburgh, ON, USA) and 1 mM L-glutamine (Gibco by Thermo Fisher Scientific; Billings, MT, USA). The medium is animal by-product-free and has similar properties to commercially available media from Sartorius [for example, 4Cell® XtraCHO Stock & Adaptation Medium (SAM)]. Cells were maintained in shake flasks with constant shaking at 130 rpm in a 37 °C incubator with 7% CO_2. Before loading on DMF devices, suspension culture aliquots were supplemented with 0.05% Tetronic 90R4 (BASF; Florham Park, NJ, USA).

Dispensing volume determination

To determine the volume and precision of the Cellspot "dispense" region, and to determine volume loss from sample loading onto pH sensing patches, droplets consisting of water, 0.05% Tetronic 90R4, and 10% food colouring dye were dispensed repeatedly, and volume was determined using image analysis in ImageJ. Electrodes of known dimensions on the device were measured to calibrate the images, and droplet perimeter measurements were converted to volume assuming a 200 μm gap height between DMF plates (based on tape thickness described above).

Cell viability assay

Dispensed test droplets containing CHO cell suspension were mixed with a 1.56 μL droplet of staining solution containing 7.5 mg mL^{-1} Hoechst 33342 (Invitrogen by Thermo Fisher Scientific) and 75.2 mg mL^{-1} propidium iodide (Sigma-Aldrich) in Dulbecco's phosphate buffered saline (Gibco) such that the final concentrations of Hoechst 33342 and propidium iodide were 5 mg mL^{-1} and 50 mg mL^{-1} respectively. Test droplets containing the stained cells were incubated on the DMF device for 10 min before capturing images on an ECLIPSE Ni fluorescent microscope (Nikon; Tokyo, Japan), by epi-exposure using brightfield, DAPI (excitation: 361–389 nm, emission: 435–485 nm), and Cy5 (excitation: 590–650 nm, emission: 662.5–737.5 nm) excitation/emission filters. Fluorescently stained nuclei were counted manually or using Fiji/ImageJ (see Macro 1 and "Supplemental Methods – Viability assay analysis" in ESI†).

Antibody quantitation using Octet® BLI system

The Octet® BLI Label-Free Detection System (Sartorius, Germany) along with the Octet® ProA Biosensor (18–5010; Sartorius, Germany) was used to measure the concentration of IgG produced by CHO DG44 cells. Different antibody concentrations yielded distinct binding rates. To establish a calibration curve, we utilized standard solutions of adalimumab biosimilar (supplied by Sartorius Stedim Cellca GmbH, Germany) at four different concentrations (10, 50, 100, and 150 μg mL^{-1}). For sensor equilibration, phosphate buffered saline (PBS; 14190-144, Thermo Fisher Scientific) was used, while sensor regeneration was achieved using 10 mM glycine (043497.22, Thermo Fisher Scientific; pH 2.0 adjusted). CHO DG44 cells grown in suspension culture (see cell culture methods above) were tested daily on the Octet® BLI system and measured values were converted to antibody concentrations in μg mL^{-1} using the calibration curve.

Fluorescence-linked immunosorbent assay (FLISA)

FLISA calibration curve assays were completed using purified IgG from human serum (I4506; Sigma-Aldrich) reconstituted in 150 mM NaCl and diluted in CHO cell medium (see Cell Culture methods above) at 0.01, 0.05, 0.1, 0.2, 0.3, 0.4, 0.5, or 0.6 g L^{-1}. Live cell assay FLISAs were completed using CHO DG44 cells (Sartorius Stedim Inc., see Cell culture methods above). All samples and reagents were mixed with Tetronic 90R4 to a final concentration of 0.05% before loading onto the DMF devices. For each Cellspot feature used, 6 μL of sample was loaded onto the device. Before FLISA assays, the cell viability assay protocol described above was completed. Hence, at the start of the FLISA assays, each test droplet contained cells or IgG standard diluted 1 : 3 with Hoechst/propidium iodide staining mixture.

Stock suspensions of superparamagnetic Dynabeads Protein A (Invitrogen by Thermo Fisher Scientific) were diluted 3-fold in SuperBlock™ (TBS) blocking buffer with 0.05% Tetronic 90R4, and 2.7 μL of the Dynabead mixture was loaded on to the small loading electrode in the Cellspot FLISA region. Beads and sample were mixed and incubated for 3 min in the DMF device using an automated protocol. After incubating beads and sample, a test droplet was retained on the device and the remainder was removed and discarded. Dynabead-containing test droplets were then mixed and incubated for 3 min with 2.7 μL of 0.04 μg mL^{-1} Rabbit Fc protein (NBP1-97061; Novus Biologicals; Littleton, CO, USA) in SuperBlock™ (TBS) blocking buffer with 0.05% Tetronic 90R4. In this step, incubation was completed on the magnet-adjacent electrodes of the FLISA region to pellet the beads at the edge of the droplet near the magnet. The remaining volume was discarded, and the beads were then washed two times with 2.35 μL droplets of SuperBlock™ (TBS) blocking buffer with 0.05% Tetronic 90R4. Dynabead-containing test droplets were then mixed and incubated for 3 min with 50 μg mL^{-1} Alexa Fluor™ 488-conjugated goat anti-human IgG (A11013; Invitrogen by Thermo Fisher Scientific) diluted in SuperBlock™ (TBS) blocking buffer with 0.05% Tetronic 90R4. The beads in a test droplet were then magnetically retained on the device and the remaining volume was discarded, and washed twice again as described above. After washing, the final test droplet was driven over the circular electrode in the FLISA testing region. Fluorescent bead-containing droplets were imaged directly on the DMF device with an ECLIPSE Ni fluorescent microscope (Nikon) by epi-exposure using brightfield and Alexa488 excitation/emission filters (Ex: 464.5–499.5 nm, Em: 516–556 nm) and a 50 ms fixed exposure time. Bead fluorescence was quantitated in Fiji/ImageJ (see Macro 2 and "Supplemental Methods – FLISA assay analysis" in ESI†).

For in-tube/pipette FLISA assays, all reagents and volumes were as described above, with the following exceptions: 1) for washing steps we used 25 μL instead of 2.35 μL, since the small volumes could not be reliably pipetted with a multi-channel pipette, 2) bead pelleting was done with a magnetic tube rack, and 3) to image the beads, 0.8 μL of bead slurry in 25 μL of wash buffer [SuperBlock™ (TBS) blocking buffer with 0.05% Tetronic 90R4] was loaded on wells of a 30-well Teflon-printed microscope slide (Electron Microscopy Sciences Inc., Hatfield, PA, USA).

pH testing

Reference pH measurements were completed using a pHenomenal MD 8000 L pH meter (VWR) using a sample volume of at least 2 mL. pH tests on DMF were completed using a PreSens pH-1 SMA HP5 optical pH probe (PreSens Precision Sensing GmbH, Regensburg, Germany). Self-adhesive pH sensors (PreSens, approx. 100 μm thick) were cut into 3/16″ diameter circular patches with a hole punch and were adhered to the top of the bottom plate of Cellspot DMF devices. The patches were positioned on the DMF device such that roughly 1.3 mm protrudes from under the edge of the top plate, so that the patch can be accessed directly with a pipette as needed. In some experiments, reagents were pipetted directly onto the sensor patches on the protruding region, allowing liquid to absorb into the patch. In other experiments, a top plate was affixed and (after carrying out other processes), droplets were actuated such that they engulfed and absorbed into the patch. In all experiments, sample was allowed to absorb into the probe for ~2 min, and then the measurement was collected by shining the PreSens optical probe through the designated window in the DMF device bottom plate. For calibration, pH standards were prepared using Dulbecco's phosphate buffered saline (Gibco) and HCl. Between measurements, the adhesive patches were cleaned by pipetting 5 μL of PBS twice, then 5 μL of UltraPure H_2O (Invitrogen) three times with drying in between using a Pasteur pipette connected to an aspirator.

Results

Design of a digital microfluidic CHO cell testing platform

We developed a bespoke DMF design for testing parameters associated with antibody-producing cell lines including antibody titre, viability, and media pH, called "Cellspot". Hereafter, we refer to Cellspot "features" to mean the 19-electrode module (Fig. 1A), and devices were configured to include six Cellspot features (Fig. 1B). The design consists of a cell mixing region with an imaging window, a dispensing region to aliquot cells for testing, a fluorescence-linked immunosorbent assay (FLISA) testing region connected to the dispensing region, a sample loading region, and an off-loading region that also serves as a loading electrode for attached pH sensing patches.

A key design-feature of Cellspot is the capacity to reproducibly dispense a sub-droplet of cell culture medium for analysis, as illustrated in Fig. 1C. In a series of design iterations leading to the version featured here, we tested a previously reported[33] "dumbbell" dispensing configuration, and compared it to dispensing with more standard square or circular shaped electrodes on the final Cellspot design (Fig. S1†). We found the "dumbbell" configurations to have excellent dispensing precision (Fig. S1A†); however, we also observed highly precise dispensing from circle and square shaped electrodes (Fig. S1B and C†). In the final device, we selected the circular design featured in Fig. 1C since it also allowed smooth droplet transitions to the surrounding electrodes (see Video file S1†). To test the precision of the dispensing electrode in our final design, dyed water was repeatedly dispensed from Cellspot features located at the top, middle, and bottom of the device, and the dispensed droplet volumes were quantified by image analysis (Fig. 1D). The mean dispensed volume was 0.78 ± 0.02 μL (ave. ± std. dev. for n = 12 replicates), with maximum error between Cellspot features of 0.026 μL and maximum error for repeated dispensing from the same feature of 0.019 μL.

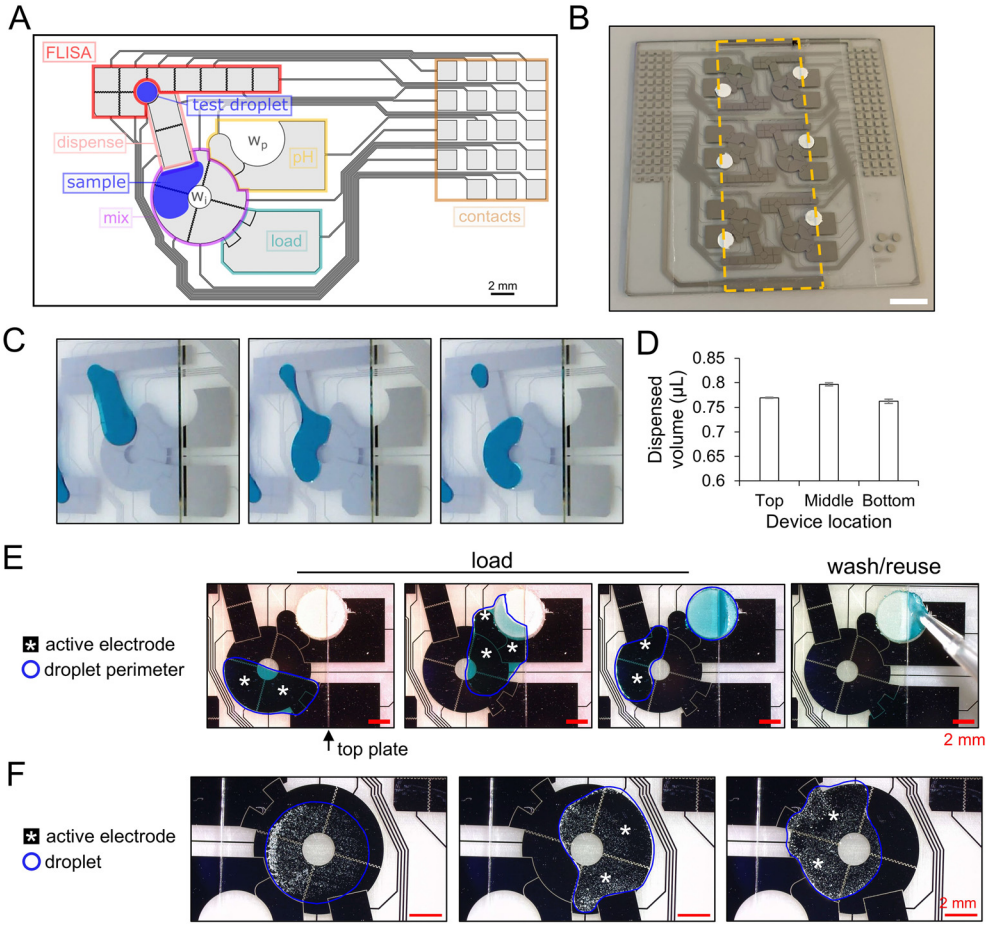

Fig. 1 Cellspot digital microfluidic device design. (A) CAD drawing of a single 19-electrode Cellspot feature, with regions dedicated to "FLISA" (red), "dispense" (salmon), "mix" (purple), "pH" (yellow), and "load" (turquoise). Each electrode is electrically connected to a designated pad in the "contacts" (brown) for interfacing with the control system. A cartoon depiction of a sample droplet (blue) that has been split to form a "test droplet" (blue) is shown. Windows in the chromium-on-glass electrodes were included in the mix region for trans-illumination imaging of cells (w_i) and the pH region for light-based pH sensing (w_p). (B) Photo of device featuring a chromium-on-glass bottom plate bearing six Cellspot features. An orange dotted line indicates the edge of the top plate substrate. The white spots are integrated pH sensors. (C) Frames from a movie illustrating the formation of a test droplet of PBS (including blue dye for visualization) using the "dispense" region. (D) Bar plot of dispensing volumes measured after dispensing from the two Cellspot features in the "top", "middle", and "bottom" on a 6× Cellspot device. Bars represent the mean of four replicates, error bars represent standard deviation. (E) Frames from a movie illustrating the Cellspot pH sensor-patch loading protocol (left) and manual washing procedure with a pipette (right). (F) Frames from a movie demonstrating resuspension of clumped CHO cells in media using the "mix" region. In (E and F) white stars indicate active electrodes and blue traces indicate the droplet perimeter.

Another key design-feature of Cellspot was the development of electrodes designed specifically to stretch droplets over a pH testing region (Fig. 1E). The design consists of two electrodes: a protruding, rounded electrode which first pulls the droplet upward, and a reservoir electrode which subsequently counter-pulls and stretches the droplet over an absorbent pH sensing patch. We tested several iterations of electrode shapes and dimensions (Fig. S2†) and found that the design shown in Fig. 1E enabled sufficient droplet stretching over the pH patch, with smoothest transitioning to the reservoir electrode. To determine the volume that absorbed into the pH patch, we loaded patches repeatedly and determined the volume loss from the initial droplet by image analysis to be 1.56 ± 0.26 µL (ave. ± std. dev. for n = 4 replicates).

A third key design-feature of Cellspot was a cell mixing region that was designed to accommodate the handling of 6–8 µL cell culture samples. Electrodes in this region were actuated in series to repetitively move the droplets around the region to imitate shake-flasks commonly used in suspension culture (Fig. 1F). In the work described here, samples were handled for short periods with mixing at ~88 revolutions per minute. In the future, these techniques will be extended to long-term cell culture.

A final key design-feature of Cellspot was the development and implementation of a user-friendly operation pipeline. Specifically, we created a digital version of the design that can be loaded into the open source MicroDrop software (Fig. S3A and B†). We also created an automated Cellspot protocol that walks the operator through each step with a series of

user prompts (Fig. S3C†), making the method convenient to teach to new users.

Cell viability assay

A key operational feature of the Cellspot system is the capacity for automated assessment of cell viability. Methods were developed to evaluate cell viability using Hoechst 33342, a blue fluorescent, cell-permeable stain and propidium iodide, a red fluorescent, cell-impermeable stain.[34] Since propidium iodide is cell impermeable, it selectively stains dead/dying cells. Hoechst 33342 and propidium iodide (PI) both fluoresce brightly when bound to DNA in the nucleus of cells, allowing nuclei to be visually identified above background fluorescence intensity in the medium.

First, we confirmed that cells stained with Hoechst 33342, PI, or both, could be visualized independently by epi-fluorescence microscopy on a digital microfluidic device (Fig. S4†). As expected, blue-fluorescent Hoechst staining was evident on all cell nuclei, and red fluorescent staining was evident on only dead cell nuclei (Fig. S4†). We then developed a digital microfluidic protocol on the Cellspot device for brief mixing of the cell suspension, automated sample dispensing, mixing with a Hoechst/PI co-staining solution, and imaging directly on the DMF device (Fig. 2A and B). To automate analysis, we wrote a macro in Fiji/ImageJ (included in ESI†) to automatically annotate and count the number of red and blue stained nuclei (Fig. 2C). Briefly, the macro uses background Hoechst fluorescence thresholding to restrict the measurement area to only the cell-containing droplet, then

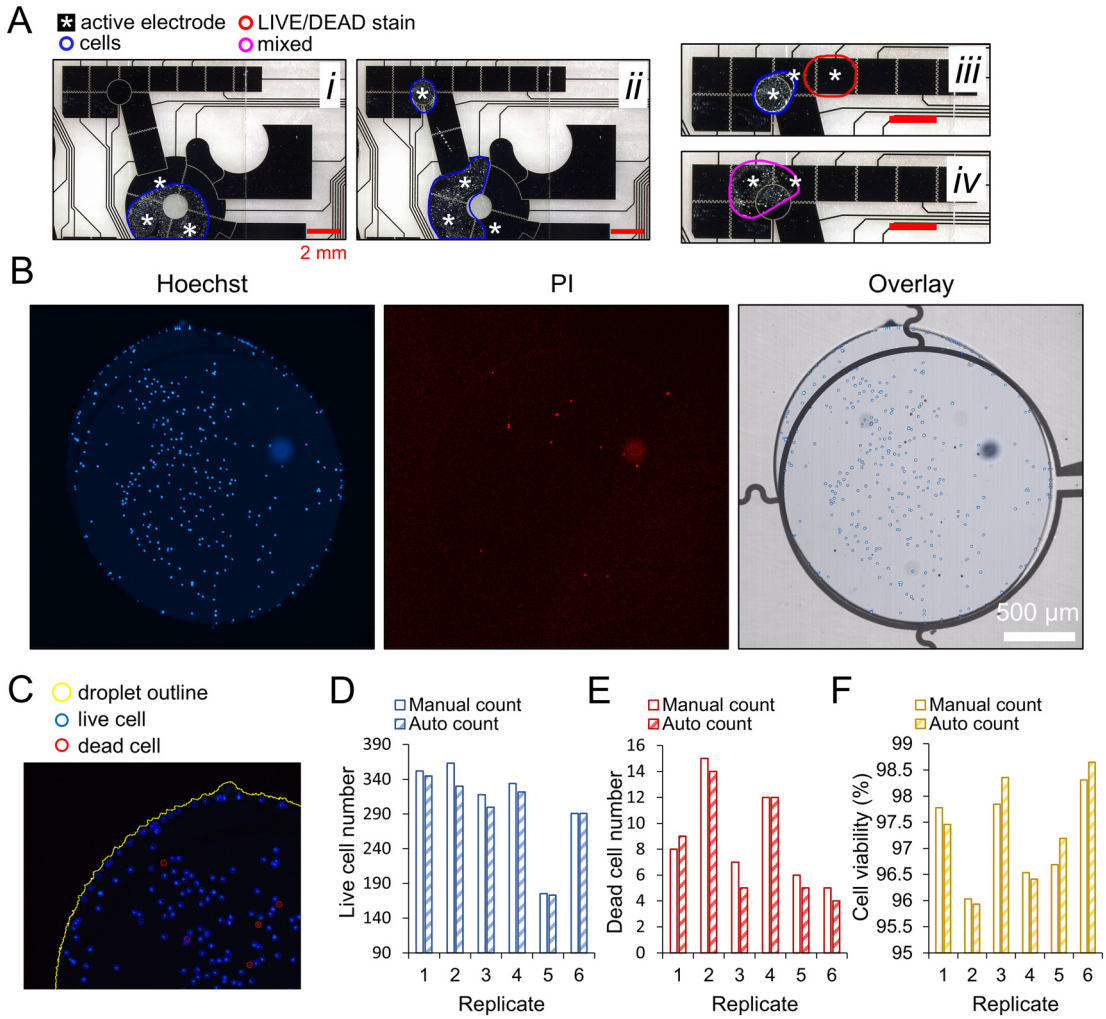

Fig. 2 Cellspot cell viability assay development. (A) Time series images (i–iv) showing dispensing of "test droplets" of CHO cell suspension and mixing with live/dead cell staining reagents. White stars indicate active electrodes. Coloured traces indicate droplet perimeter. Blue traces indicate cell-containing droplets, red trace indicates live/dead stain-containing droplet, and magenta trace indicates mixed droplet. (B) Epifluorescence microscopy images of CHO cells on a Cellspot device stained with Hoechst (live cells, left) and propidium iodide (PI; dead cells, middle), overlaid on bright field (right) using the automated DMF protocol. (C) Visual representation of Fiji/ImageJ automated analysis of live/dead stained CHO cell images. The droplet perimeter is highlighted in yellow, counted live cells are encircled in blue, and counted dead cells are encircled in red. (D–F) Plots of live/dead cell counts and percentages using Fiji/ImageJ (hatched bars) or manual counting (open bars), n = 6 replicates, including (D) live (Hoechst) cell counts, (E) dead (propidium iodide) cell counts, and (F) cell viability based on live/dead cell counts.

uses a local maxima-finding function to count the number of red- and blue-stained nuclei within the droplet. To establish the accuracy of the automated counting macro, we repeated the cell staining assay six times on a Cellspot device and counted the number of live and dead cells both manually and using the Fiji/ImageJ macro (Fig. 2D and E). Cell viability under these conditions was high, with 97.2 ± 0.9% (mean ± std. dev.) viability, and we found close agreement between both viability estimates, with a maximal discrepancy in estimated cell viability of 0.51% and a discrepancy of manual relative to automated counts of 0.32 ± 0.18% (mean ± std. dev.) (Fig. 2F).

Fluorescence-linked immunosorbent assay (FLISA)

A third key operational feature of the Cellspot system is the capacity to assay mAb production levels. We chose to use a magnetic-bead-based system immunoassay for this purpose, building from methods reported previously.[26,28,35] Pelleting and washing of beads can be accomplished within a DMF device using either a movable magnet on a motorized stage,[28,35] or with a stationary magnet for asymmetrical splitting.[26] Here we adopted the latter method (Fig. 3A) since it requires fewer integrated parts, which will (in future work) make it straightforward to integrate the entire Cellspot device inside a fluorescent microscope. First, we tested the position of the magnet by securing small rectangular magnets above or below the DMF device at varying positions relative to the testing region on the Cellspot device (Fig. S5A†). We observed that a magnet positioned 1.31 mm horizontally from the bead-containing droplet (Fig. 3B) and below the device could pellet the majority of beads within 3 min (Fig. 3C). For convenience, we designed and fabricated a plastic slider that can be used to position six magnets under each of the Cellspot features in in a standard Sci-Bots Dropbot instrument (Fig. S5B and C†). We also confirmed that beads and fluorescence from a bound AlexaFluor488-conjugated antibody could be imaged directly on the device using epifluorescence microscopy (Fig. 3D). Finally, we tested whether imaging of the fluorescent beads over chromium

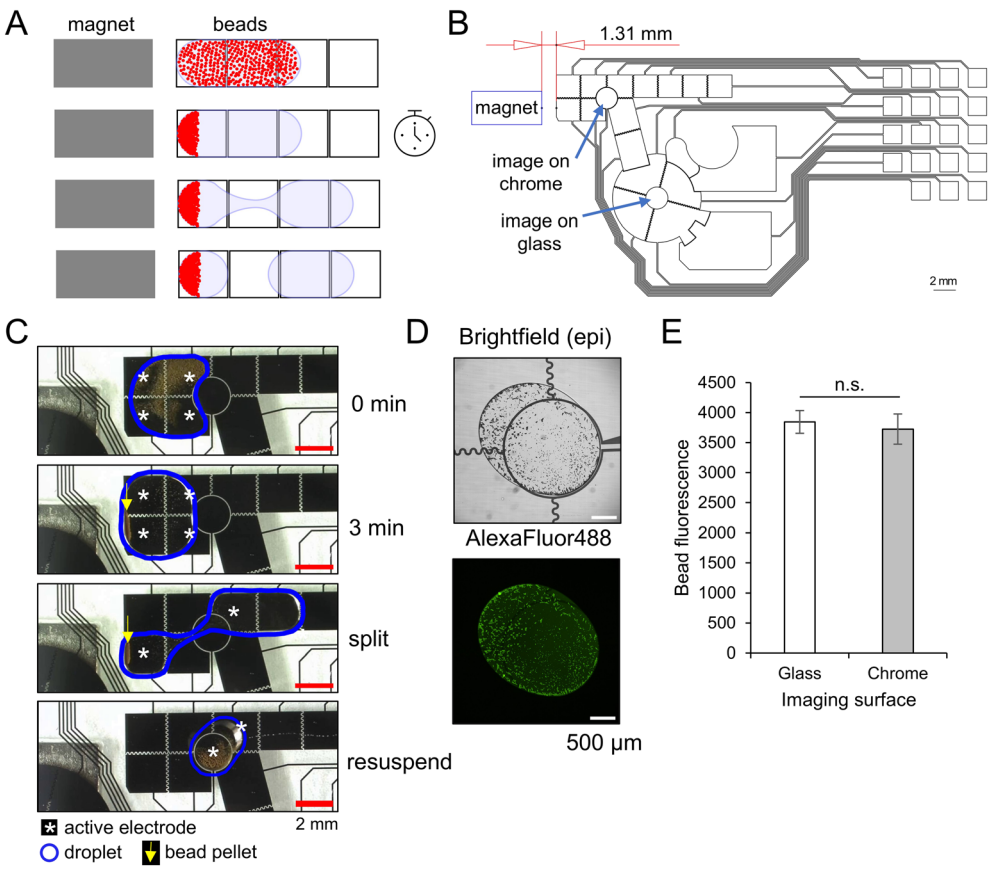

Fig. 3 Magnetic bead pelleting and imaging on the Cellspot DMF device. (A) Cartoon representation (top-to-bottom) of the asymmetrical splitting of magnetic particles (red) method from a droplet (blue). (B) CAD drawing of magnet (open blue box) orientation relative to the Cellspot FLISA region, with labels pointing to device locations used for bead imaging. (C) Time series images (top-to-bottom) of magnetic bead pelleting, sub-droplet retention, and bead resuspension using an automated DMF protocol. White stars indicate active electrodes. Blue traces indicate droplet perimeter. Yellow arrows point to magnetic bead pellet at droplet periphery. (D) Epi-illumination microscopy images of magnetic beads (top: bright-field, bottom: fluorescent) with bound AlexaFluor88-conjugated antibodies positioned in the FLISA region of a Cellspot DMF device. (E) Plot of bead fluorescence measured from magnetic beads with bound fluorescent antibodies collected from droplets positioned on glass (left) *versus* chromium (right). *N* = three replicates, error bars indicate standard deviation. n.s. = not significant according to independent sample *t*-test.

electrodes or glass windows (wherein chromium is etched from the device surface; w_i in Fig. 1A) was more appropriate, and observed no difference in fluorescent signal between glass and chromium (Fig. 3E). Hence, all subsequent images used for bead fluorescence quantitation were captured from droplets positioned on chromium electrodes.

Armed with a method for reproducibly separating magnetic particles in the Cellspot system, we developed a magnetic bead-based FLISA for detecting human IgG (as a proxy for mAb produced by cultured cells) in samples on DMF. The assay used paramagnetic Dynabeads modified with protein A to capture antibodies in the sample (Fig. 4A). Fc protein from rabbit was then used to block unoccupied protein A sites on the beads, and the sample antibody was detected using an AlexaFluor488-conjugated, cross-adsorbed anti-human IgG secondary antibody (Fig. 4A). Since the Fc blocking protein is sourced from rabbit and the secondary antibody is cross-adsorbed against rabbit serum, we expected the secondary antibody to bind specifically to the human IgG sample antibody and not the Fc blocking protein. This was supported by our observation that fluorescent signal on the beads was negligible in the absence of a sample antibody, and increasing concentration of human IgG standard in the sample produced increasing bead fluorescence (Fig. 4B). We quantitated the assays using a Fiji/ImageJ macro (see ESI† appendix). Briefly, the macro uses thresholding to annotate areas of the image containing fluorescing beads, then measures the fluorescence of individual beads or small cluster of beads in terms of units per area (Fig. 4C). Compared to bulk fluorescence measurements, this approach yields higher signal to noise and is not sensitive to variability in bead retention numbers. The latter assertion was tested by plotting the total area of analyzed beads against the mean fluorescence per bead area for several IgG concentrations (Fig. 4D). Importantly, we did not observe a correlation between the number of beads retained in the quantitated

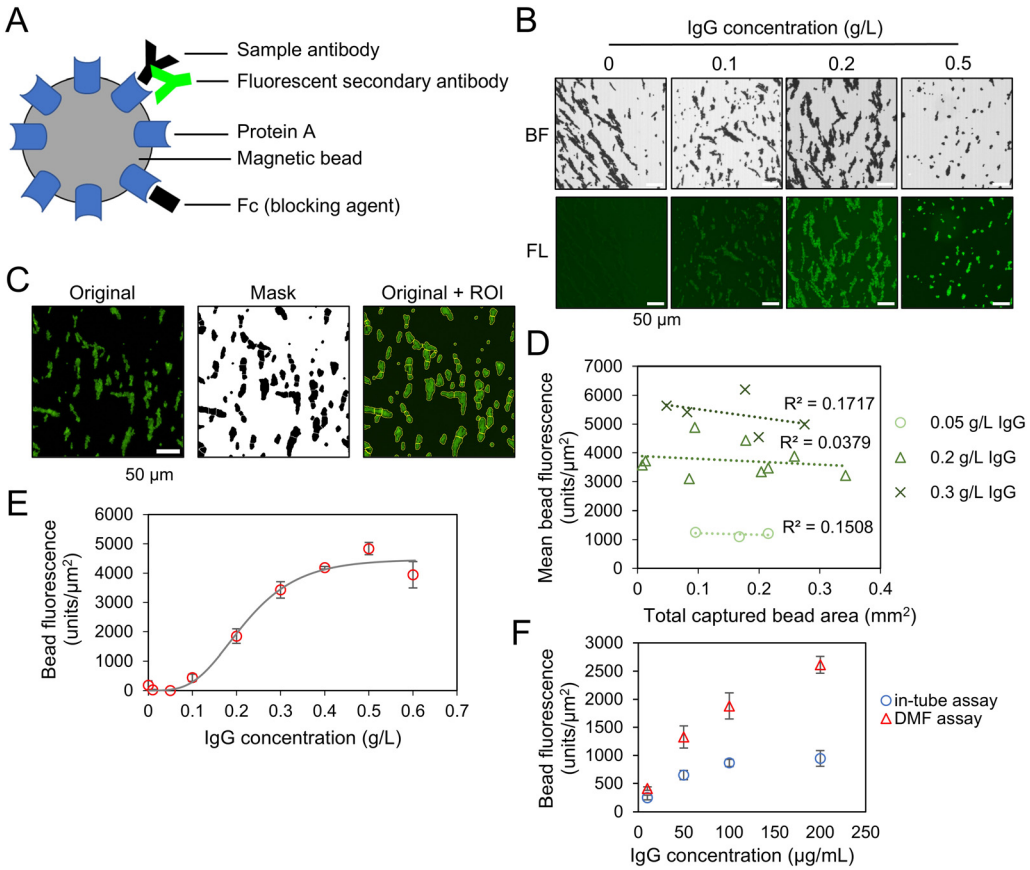

Fig. 4 Cellspot FLISA development. (A) Cartoon representation of the antibody detection FLISA assay. (B) Epi-illumination microscopy images (top: bright-field; bottom: fluorescence) of magnetic beads with bound fluorescent antibody after running FLISA assays on a Cellspot DMF device after exposure to increasing (left-to-right) human IgG concentrations. (C) Visual representation of Fiji/ImageJ bead fluorescence analysis. Starting with an original image (left), thresholding was used to generate a mask (middle) to annotate single beads or clusters of beads using ImageJ region of interest (ROI) annotations (right). (D) Scatter plots of relationship between bead area and mean fluorescence from Cellspot-automated FLISA assays performed with 0.05 g L^{-1} (circles), 0.2 g L^{-1} (triangles), or 0.3 g L^{-1} ('x's) of sample antibody. Individual markers represent independent replicates, and dotted lines represent linear model fits to the different IgG concentrations with Pearson R^2 correlation coefficients labelled. (E) On-DMF calibration curve data (red circles) of FLISA signal as a function of IgG concentration with non-linear model fit. Data points represent the mean of at least three independent replicates and error bars represent standard deviation. (F) In-tube (blue circles) *versus* DMF (red triangles) FLISA comparison. Data points represent the mean of at least three independent replicates and error bars represent standard deviation.

images and the observed fluorescence, indicated by the near-zero R^2 coefficients from linear fits to the data (Fig. 4D).

After initial development of the Cellspot FLISA method, we evaluated the following questions: (i) whether it had an appropriate dynamic range for the targeted application, (ii) the suitability of the standard used for calibration of the assay, and (iii) how the DMF method compared with similar methods performed in tubes. To address question (i), we measured IgG production over a three-day time-course from a CHO-DG44 cell line (which is known to generate an Adalimumab biosimilar human IgG) using a biolayer interferometry (BLI) assay. We observed that after three days of culture, the cells produced signal equivalent to 125.7 ± 5.3 μg mL^{-1} IgG (ave. ± std. dev.; Fig. S6A†). This level of production was found to be a good match for the Cellspot DMF FLISA, which had a range of 0.1–0.4 g L^{-1} IgG (Fig. 4E). To address question (ii) – the suitability of the standard used for calibration – we repeated the assay using purified Adalimumab or human IgG standard at the same concentration (0.4 g L^{-1}). We did not observe a significantly different signal using IgG standard compared to adalimumab (Fig. S6B†), confirming that generic human IgG can be used to calibrate the assay. Finally, to address question (iii) – a comparison of the performance of the Cellspot DMF FLISA to similar methods performed in tubes – we completed the DMF-scaled assay in tubes using a magnetic rack to pellet beads, and volumes equivalent to our DMF protocol (Fig. 4F). As shown, the Cellspot assay seems to have higher sensitivity; however, we suspect that this does not reflect a fundamental difference between the two systems, and that the assay conditions can be optimized for different volumes and systems depending on the application. Regardless, in sum, a sensitive on-chip detection method was developed and demonstrated to be useful for quantifying mAb production in cell culture.

Media pH assay

A fourth key operational feature of the Cellspot system is the capacity to measure pH *in situ*, during cell culture and analysis. To measure droplet pH inside a DMF device, we tested an optical pH sensor that uses analytical sensing patches adhered to glassware. pH sensing patches were adhered to the DMF bottom plate over the w_p window in the Cellspot design (Fig. S7A and B†). A method was developed to allow for a droplet on the Cellspot device to be loaded onto the pH sensor (Fig. 1E and S2†). Prior to conducting experiments, the PreSens pH meter was calibrated using PBS standards in the 5.9–8.0 pH range (Fig. 5A). Conveniently, we found no difference in observed pH when the patch was completely covered by a DMF top plate *versus* partially covered (Fig. S7C and D†). This allowed us to position the patch with a protruding edge beyond the top plate, such that the sensor patch can be washed and reused by pipetting (Fig. 1E, right).

After initial development of the on-DMF pH sensing approach, we evaluated the following questions: (i) whether

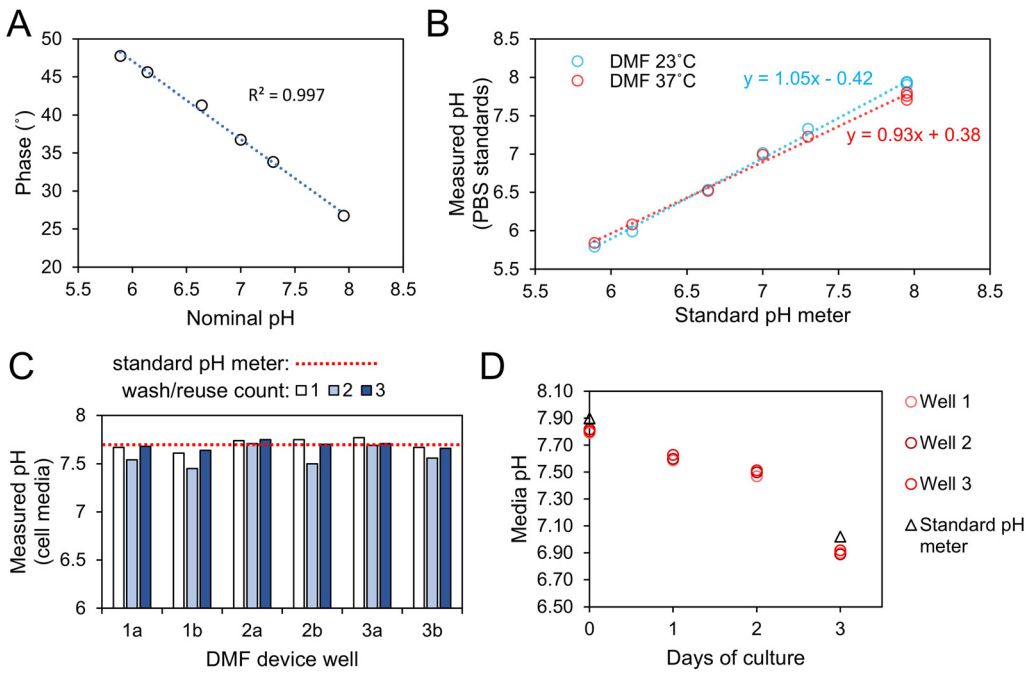

Fig. 5 Cellspot pH assay development. (A) Calibration curve (open circles) generated using PreSens pH meter with known pH droplets on a PreSens pH patch adhered to a Cellspot DMF device, with dashed line of regression. (B) Temperature effect with pH patches loaded at 23 °C or in 37 °C incubator. Blue (23 °C) and red (37 °C) lines depict observed regressions on DMF. (C) CHO cell media pH measured after repeated washing and reuse (1x-white, 2x-lt. blue, 3x-drk. blue) of pH patches on each of the six replicate features (1a–b, 2a–b, 3a–b) of a Cellspot DMF device. Dotted red line represents the measured pH using a standard pH meter. (D) Live cell culture pH measurements. Shades of red/pink circles indicate biological replicates. Black triangles indicate measurements form standard pH meter on day 0 and day 3.

the measured pH was influenced by temperature (since the eventual goal is to operate this device inside an incubator), (ii) whether readings are stable after repeated washing and reuse of the sensor patches, (iii) whether accurate readings could be attained from samples containing live cells in culture media. To address question (i) we tested pH of PBS standards loaded inside a 37 °C incubator using DMF. We observed a small but significant (p = 0.004) under-reading of −0.17 ± 0.03 pH for the pH 7.95 standard at 37 °C, but did not observe a notable shift in readings for the other standards (Fig. 5B). To address question (ii) – reading stability after washing and reuse – we repeatedly measured the pH of cell culture media on each of the six sensors adhered to a Cellspot DMF device, and washed and dried them between measurements (Fig. 5C). In these experiments, the cell culture media pH was 7.7 (according to a standard pH meter) and the mean reading measured *in situ* on the Cellspot device was 7.66 ± 0.09 (ave. ± std. dev.), with a maximal discrepancy between readings of 0.32. To address question (iii) – accuracy for cell-containing samples – we cultured CHO cells in well plates for three days and measured pH by loading samples on DMF inside an incubator daily. On the first and last day we measured samples from the same cultures using a standard pH meter. We observed an expected reduction in media pH over time from cell metabolism,[36] and readings using the integrated sensor were close to the standard meter readings on the outset and completion of the experiment (Fig. 5D).

In sum, the new method can reliably measure the pH of small-volume droplets on a digital microfluidic device. In the procedure described here, approximately 25% of the droplet (and cells within it) is used for each measurement, such that the remaining 75% can be kept for additional culture. In future work, different ratios will be explored for long-term, repeated measurements.

Live cell multimodal assay: viability, pH, and IgG production

After developing and optimizing each of the operational features of the Cellspot DMF method, we were ready to apply it to its full application – integrated viability assays, pH monitoring, and analysis of antibody production. We captured a video of the entire multi-assay procedure using human IgG diluted in cell culture media to demonstrate the complete protocol (Video file S1†). In total, the entire multi-assay takes an average of ~40 min to complete, and each assay is completed sequentially, starting with pH measurement, followed by the viability assay, and finally the FLISA assay. For the live-cell experiment, we used samples of a mAb-producing cell line to test the media pH, cell viability, and mAb productivity of each culture daily. Assays were initiated one hour after defrosting cells from storage in liquid nitrogen, to visualize the recovery process from defrosting to observable production of the expressed antibody. We selected a three-day time-course, since standard culturing guidelines recommend passaging cells every three days. Thus, the cell density in this timeframe was representative of a normal range of culturing density. For cell viability and IgG production experiments, a single 6 μL droplet of cell suspension was loaded onto the DMF device, which was dispensed from and assayed in the FLISA region (Fig. 1A; see Video file S1†).

Cell viability assay results revealed an expected lower initial viability immediately after thawing the cells of 79 ± 3% (ave. ± std. dev.) viability, and a gradual recovery to 98 ± 2% (ave. ± std. dev.) viability by day 3 (Fig. 6A and B). Importantly, we did not observe over-crowding of the culture in this timeframe, and thus accurate viability counts could be collected throughout the experiment. The media pH measurements indicated an initial rise in pH from 7.60 ± 0.06 (ave. ± std. dev., day 0) to 7.73 ± 0.04 (ave. ± std. dev., day 1) (Fig. 6C), likely from the media acclimating to the elevated CO_2 levels in the incubator. On days 2 and 3, we observed a reduced but stable pH of 7.41 ± 0.07 (ave. ± std. dev., day 2) and 7.40 ± 0.04 (ave. ± std. dev., day 3) respectively (Fig. 6C), consistent with the known pH-reducing effect of mammalian cells in culture.[36] For IgG concentration FLISA measurements, we used the human IgG protein standard curve (Fig. 4E) to convert observed fluorescence values to IgG concentrations. After 2 days in culture, we observed an IgG concentration of 132 ± 9 μg mL^{-1} (ave. ± std. dev.), which increased to 223 ± 18 μg mL^{-1} (ave. ± std. dev.) on day 3 (Fig. 6D and E). In sum, three assays associated with cell growth and productivity (viability, media pH, and antibody productivity) were automated on a single platform, using less than ten microlitres of culture sample for each replicate multi-assay.

Discussion

Cell culture on digital microfluidics

There is a long history of using DMF to culture mammalian cells, including adherent cell lines,[24,25,37,38] suspension cell lines,[29] primary cells,[39] and 3D cell constructs.[40–47] These systems have been demonstrated to be capable of automated, multi-day cell culture, in some cases including automated passaging techniques.[48] The work presented here builds on these key innovations; however, we did not focus on multi-day culture in DMF. Rather, in the proof-of-concept results presented here, cells were cultured in flasks in incubators, and then transferred to DMF devices for experiments, featuring on-chip viability measurements. The novelty reported here is the combination of cell culture with analysis of cell viability, mAb production, and with in-line pH measurements.

Small volume ELISA/FLISA on digital microfluidics

Many microfluidic platforms have been developed for the purpose of automated immunoassays,[49] including digital microfluidics (DMF) for bead-based ELISAs[26,28,35] (similar to the approach described here). Compared to pipetting, DMF can more precisely manipulate microliter to sub-

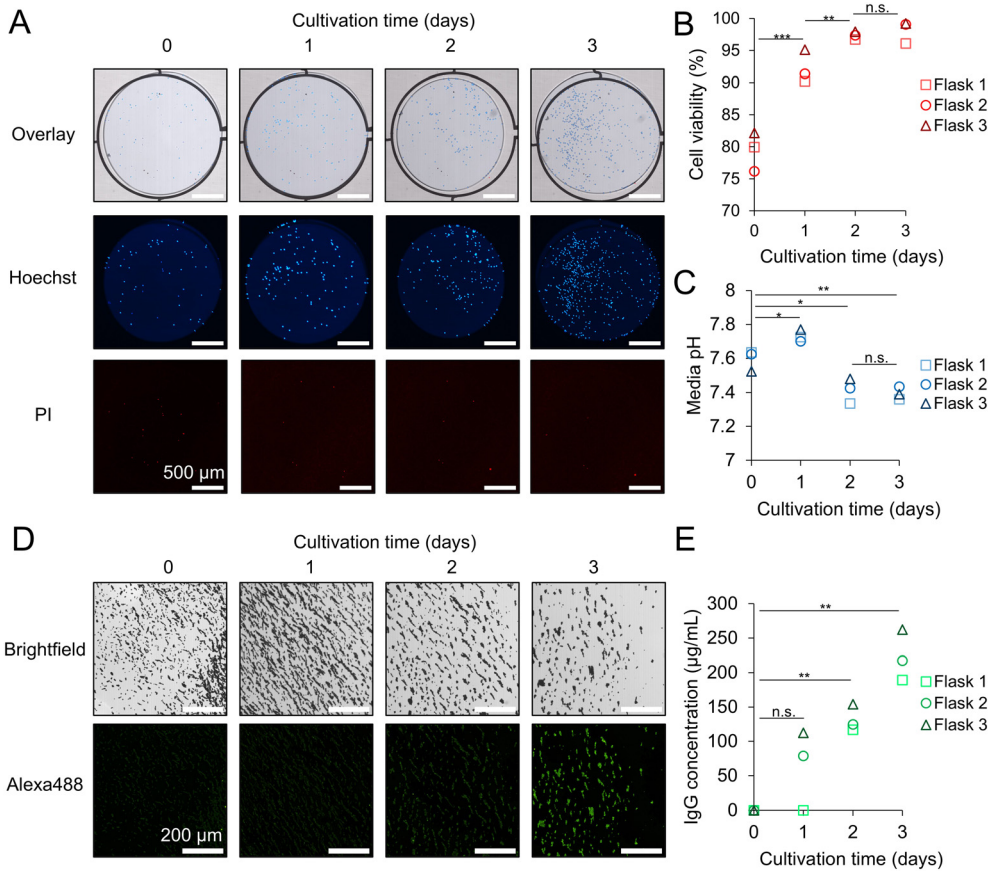

Fig. 6 Automated CHO cell multi-assay on a Cellspot DMF device. Multi-parametric assay results from culturing three independent flasks of human IgG-expressing CHO cells and testing with automated Cellspot DMF protocols. (A) Epi-illumination microscopy images (brightfield/overlay-top; Hoechst-middle, PI-bottom) collected during viability assays. Plots of (B) cell viability and (C) cell media pH as a function of cultivation time. (D) Epi-illumination microscopy images (brightfield-top, Alexa488-bottom) of bead suspensions collected during human IgG FLISA assays. (E) Plot of human IgG FLISA assay results as a function of cultivation day. Markers (square, circle, triangle) indicate independent measurements from different flasks of cells. Stars depict statistically significant differences based on independent sample *t*-tests (n.s. not significant, * $p < 0.05$, ** $p < 0.01$).

microliter droplets. DMF also uses anti-fouling coatings on the interior surfaces of devices (fluoropel or Teflon), and an anti-fouling surfactant (Tetronic 90R4),[50] which reduces protein adsorption onto surfaces. Here we found that both DMF-based and pipetting-based approaches to our bead-based FLISA assay could produce reliable and quantitative readouts of antibody production. However, the DMF approach was more convenient when using small volumes of sample (0.7–5 µL), since bead manipulation steps are automated. A key innovation of the assay developed here was the use of fluorescence microscopy to measure localized, on-bead fluorescence (in contrast to conventional schemes that measure average luminescence in bulk fluid[6,28,35]), which made our system highly tolerant to common challenges with bead-based ELISA/FLISA assays including variability in bead aggregation and variability in bead retention numbers. In terms of sample consumption, our approach is competitive with spectroscopy methods that can measure antibody titres and cell viability from 2 µL of CHO cell supernatant,[51] since only 0.78 µL dispensed droplets of sample were used for both the FLISA and cell viability assays.

Channel-based microfluidic devices have been reported specifically for measuring IgG production titres from antibody-producing mammalian cell lines.[18–21] However, to our knowledge this is the first reported example of this application specifically on DMF. A unique challenge in detecting IgG production from cell lines is that the analyte is present at high concentrations, typically in the range of ~50–1000 µg mL^{-1}. For this reason, we did not extensively characterize the lower limit of detection of our DMF FLISA assay, and rather developed an assay that would capture a suitable range of concentrations for the cell line used in our study. In this case our quantitative range was ~4-fold, from 100–400 µg mL^{-1}, using a dispensed sample volume of 0.78 µL. Others have achieved comparable or broader detection ranges in channel-based microfluidic devices, but from larger sample volumes. For example, Pinto *et al.*[18] reported an ~9-fold range of ~10–90 µg mL^{-1} from a 51 µL sample (based on reported 1.7 µg mL^{-1} flow rate for 30 min), and Rohskopf *et al.*[20] reported an ~4.6-fold range of 6.88–31.77 nM (or ~1.03–4.77 µg mL^{-1} assuming a typical IgG molecular

weight of 15 kDa) from a continuous flow device using an unreported volume of analyte. Hence, our quantitative range of ~4-fold is narrower than some reported microfluidic methods, but requires ~65-fold less sample volume. For this reason, we envision that our platform will be well suited for characterizing cell lines early in the expansion process from single cell isolates, when culture volumes are a limiting factor.

Optical pH sensing on digital microfluidics

Accurate pH sensing within a digital microfluidic device represents a significant challenge. Sophisticated and highly sensitive methods based on electrochemistry have been implemented in microchannel-based and/or droplet microfluidic devices;[52–54] however, we envisioned that incorporation of electrochemical sensing elements into the Cellspot device would complicate fabrication and increase cost-per-device. Another approach uses pH-sensitive dyes or nanoparticles added to droplets, which change color or fluorescence on pH changes.[55–58] We chose to avoid these approaches (which involved adding a reagent to culture samples), since in initial testing, limits on metering made it challenging to avoid perturbing the pH of our <10 μL sample droplets. Thus, in this work, we chose to work with a solid-phase optical pH sensor (PreSens Precision Sensing GmbH, Regensburg, Germany), as it was found to be compatible with the DMF system. Another report used a solid-phase optical sensor to measure dissolved oxygen in bacterial cultures on DMF,[59] and others have used solid-phase pH sensors in channel microfluidic devices.[60] However, to our knowledge there are no previous reports of using this type of sensor for pH measurement in DMF systems, and certainly not in combination with cell culture, viability, and mAb measurements.

To operationalize the optical pH sensor in Cellspot, we developed a novel electrode configuration to stretch droplets over the absorptive pH sensing patches. This was done to avoid adhering the sensor patches directly to electrodes, which can risk damaging the dielectric layer above electrodes when actuated. For convenience, we found that the patch could be positioned with partial coverage from the top plate. This did not affect measurements and allowed us to easily access the adhered optical sensing patch to wash and reuse it. We envision that this approach of stretching droplets over adhered optical patches on DMF could be expanded to other optical sensing patches. Indeed, others have developed optical sensing patches for diverse cell culture analytes, including dissolved oxygen,[61] carbon dioxide,[62] and glucose.[63] Hence, the approach described here opens future opportunities for detecting other important cell culture analytes on DMF.

Limitations of the digital microfluidic testing platform

As with any new microfluidic system, there are limitations of Cellspot. First, we have not yet integrated the Cellspot with automated imaging and reagent loading capabilities. However, the use of optical sensing for all of the described assays and the electronic nature of DMF should allow seamless integration with these capabilities in future iterations. Indeed, we and others have demonstrated the integration of optical sensing in a DMF system in numerous other applications (reviewed recently in ref. 64). Another limitation is throughput, given that our device can only run six independent experiments simultaneously. However, the ~40 min run-time of the assay means that numerous assays can be completed in a single day, and the DMF devices can easily be washed and re-used for sequential experiments. Further, the operating unit (DropBot) used is relatively inexpensive and occupies a small footprint on a benchtop (10 × 15 cm), meaning that labs could be equipped with multiple units to increase throughput.

Finally, a long-standing limitation of DMF is fabrication, since devices are typically fabricated in a clean room with specialized equipment. However, simpler and more cost-effective DMF device fabrication methods are a highly active area of investigation.[65–68] Meanwhile, increasing commercialization of DMF platforms, further incentivized by the demonstration of high value-to-industry applications as shown here, should continue to motivate the improvement of DMF fabrication capabilities.

Conclusions

We have reported a semi-automated digital microfluidic platform for testing cell viability, antibody production titres, and media pH of antibody-producing cells. The device can perform each of these assays using less than ten microlitres of cell culture in one integrated platform, minimizing the sample and reagent requirements needed for early-stage testing of recombinant cell lines. We anticipate that this technology will become a convenient tool in the cell line development toolbox once it has been fully integrated with automated imaging and optical sensing.

Data availability

Two custom Fiji/ImageJ macros were developed to support this manuscript. The macros are included as a part of the ESI† submitted along with the manuscript. The raw data associated with this manuscript is available from the corresponding author upon request.

Author contributions

Lant, J. T.: conceptualization, data curation, formal analysis, investigation, methodology, project administration, software, resources, visualization, writing – original draft. Frasheri, J.: conceptualization, investigation, methodology. Kwon, T.: investigation, validation, resources, writing – review & editing. Tsang, C. M. N.: formal analysis, software. Li, B. B.: conceptualization, methodology. Decombe, S.: conceptualization, methodology. Sklavounos, A. A.:

methodology. Akbari, S.: conceptualization, funding acquisition, project administration, writing – review & editing. Wheeler, A. R.: conceptualization, funding acquisition, project administration, resources, supervision, writing – review & editing.

Conflicts of interest

J. T. Lant, J. Frasheri, S. Akbari, S. Decombe, and A. R. Wheeler are inventors on a patent application related to some aspects of the work presented here, and T. Kwon and S. Akbari are employed by one of the sponsors of the project.

Acknowledgements

The work in this manuscript was supported by funding from the National Science and Engineering Research Council of Canada (NSERC ALLRP 559533 – 20) and from Sartorius Stedim North America. We are grateful to Dr. Ian Swyer, Dr. Michael Dryden and Dr. Dean Chamberlain for critical advice on experimental methods.

References

1 R. J. Kaufman, L. C. Wasley, A. J. Spiliotes, S. D. Gossels, S. A. Latt and G. R. Larsen, *et al.*, Coamplification and coexpression of human tissue-type plasminogen activator and murine dihydrofolate reductase sequences in Chinese hamster ovary cells, *Mol. Cell. Biol.*, 1985, **5**(7), 1750–1759.
2 D. M. Ecker, S. D. Jones and H. L. Levine, The therapeutic monoclonal antibody market, *mAbs*, 2015, **7**(1), 9–14.
3 The Antibody Society [Internet], [cited 2023 Mar 31], Antibody therapeutics product data, available from: **https://www.antibodysociety.org/antibody-therapeutics-product-data/**.
4 R. M. Lu, Y. C. Hwang, I. J. Liu, C. C. Lee, H. Z. Tsai and H. J. Li, *et al.*, Development of therapeutic antibodies for the treatment of diseases, *J. Biomed. Sci.*, 2020, **27**(1), 1.
5 A. Frenzel, M. Hust and T. Schirrmann, Expression of recombinant antibodies, *Front. Immunol.*, 2013, **4**, 217.
6 R. Jefferis, Glycosylation of Recombinant Antibody Therapeutics, *Biotechnol. Prog.*, 2008, **21**(1), 11–16.
7 M. C. Glassy, J. P. Tharakan and P. C. Chau, Serum-free media in hybridoma culture and monoclonal antibody production, *Biotechnol. Bioeng.*, 1988, **32**(8), 1015–1028.
8 W. Li, Z. Fan, Y. Lin and T. Y. Wang, Serum-Free Medium for Recombinant Protein Expression in Chinese Hamster Ovary Cells, *Front. Bioeng. Biotechnol.*, 2021, **9**, 646363.
9 J. H. Zhang, L. L. Shan, F. Liang, C. Y. Du and J. J. Li, Strategies and Considerations for Improving Recombinant Antibody Production and Quality in Chinese Hamster Ovary Cells, *Front. Bioeng. Biotechnol.*, 2022, **10**, 856049.
10 I. Hernandez, S. W. Bott, A. S. Patel, C. G. Wolf, A. R. Hospodar and S. Sampathkumar, *et al.*, Pricing of monoclonal antibody therapies: higher if used for cancer?, *Am. J. Manag. Care.*, 2018, **24**(2), 109–112.
11 F. M. Wurm, Production of recombinant protein therapeutics in cultivated mammalian cells, *Nat. Biotechnol.*, 2004, **22**(11), 1393–1398.
12 N. K. Hamaker and K. H. Lee, Site-specific integration ushers in a new era of precise CHO cell line engineering, *Curr. Opin. Chem. Eng.*, 2018, **22**, 152–160.
13 W. Yang, J. Zhang, Y. Xiao, W. Li and T. Wang, Screening Strategies for High-Yield Chinese Hamster Ovary Cell Clones, *Front. Bioeng. Biotechnol.*, 2022, **10**, 858478.
14 X. Pan, M. Streefland, C. Dalm, R. H. Wijffels and D. E. Martens, Selection of chemically defined media for CHO cell fed-batch culture processes, *Cytotechnology*, 2017, **69**(1), 39–56.
15 K. Paul, T. Hartmann, C. Posch, D. Behrens and C. Herwig, Investigation of cell line specific responses to pH inhomogeneity and consequences for process design, *Eng. Life Sci.*, 2020, **20**(9–10), 412–421.
16 D. Reinhart, L. Damjanovic, C. Kaisermayer, W. Sommeregger, A. Gili and B. Gasselhuber, *et al.*, Bioprocessing of Recombinant CHO-K1, CHO-DG44, and CHO-S: CHO Expression Hosts Favor Either mAb Production or Biomass Synthesis, *Biotechnol. J.*, 2019, **14**(3), 1700686.
17 T. Hogiri, H. Tamashima, A. Nishizawa and M. Okamoto, Optimization of a pH-shift control strategy for producing monoclonal antibodies in Chinese hamster ovary cell cultures using a pH-dependent dynamic model, *J. Biosci. Bioeng.*, 2018, **125**(2), 245–250.
18 I. F. Pinto, R. R. G. Soares, M. E. L. Mäkinen, V. Chotteau and A. Russom, Multiplexed Microfluidic Cartridge for At-Line Protein Monitoring in Mammalian Cell Culture Processes for Biopharmaceutical Production, *ACS Sens.*, 2021, **6**(3), 842–851.
19 T. Kwon, S. H. Ko, J. F. P. Hamel and J. Han, Continuous Online Protein Quality Monitoring during Perfusion Culture Production Using an Integrated Micro/Nanofluidic System, *Anal. Chem.*, 2020, **92**(7), 5267–5275.
20 Z. Rohskopf, T. Kwon, S. H. Ko, D. Bozinovski, H. Jeon and N. Mohan, *et al.*, Continuous Online Titer Monitoring in CHO Cell Culture Supernatant Using a Herringbone Nanofluidic Filter Array, *Anal. Chem.*, 2023, **95**(39), 14608–14615.
21 K. Van Manen-Brush, J. Zeitler, J. R. White, P. Younge, S. Willis and M. Jones, Improving Chinese hamster ovary host cell protein ELISA using Ella ® : an automated microfluidic platform, *BioTechniques*, 2020, **69**(3), 186–192.
22 A. H. C. Ng, B. B. Li, M. D. Chamberlain and A. R. Wheeler, Digital Microfluidic Cell Culture, *Annu. Rev. Biomed. Eng.*, 2015, **17**, 91–112.
23 L. Pang, J. Ding, X. X. Liu and S. K. Fan, Digital microfluidics for cell manipulation, *TrAC, Trends Anal. Chem.*, 2019, **117**, 291–299.
24 A. B. V. Quach, S. R. Little and S. C. C. Shih, Viral Generation, Packaging, and Transduction on a Digital Microfluidic Platform, *Anal. Chem.*, 2022, **94**(9), 4039–4047.
25 S. C. C. Shih, I. Barbulovic-Nad, X. Yang, R. Fobel and A. R. Wheeler, Digital microfluidics with impedance sensing for

integrated cell culture andanalysis, *Biosens. Bioelectron.*, 2013, **42**, 314–320.
26 R. Sista, Z. Hua, P. Thwar, A. Sudarsan, V. Srinivasan and A. Eckhardt, *et al.*, Development of a digital microfluidic platform for point of care testing, *Lab Chip*, 2008, **8**(12), 2091.
27 A. H. C. Ng, R. Fobel, C. Fobel, J. Lamanna, D. G. Rackus and A. Summers, *et al.*, A digital microfluidic system for serological immunoassays in remote settings, *Sci. Transl. Med.*, 2018, **10**(438), eaar6076.
28 A. H. C. Ng, K. Choi, R. P. Luoma, J. M. Robinson and A. R. Wheeler, Digital Microfluidic Magnetic Separation for Particle-Based Immunoassays, *Anal. Chem.*, 2012, **84**(20), 8805–8812.
29 S. H. Au, R. Fobel, S. P. Desai, J. Voldman and A. R. Wheeler, Cellular bias on the microscale: probing the effects of digital microfluidic actuation on mammalian cell health, fitness and phenotype, *Integr. Biol.*, 2013, **5**(8), 1014.
30 D. G. Rackus, M. D. M. Dryden, J. Lamanna, A. Zaragoza, B. Lam and S. O. Kelley, *et al.*, A digital microfluidic device with integrated nanostructured microelectrodes for electrochemical immunoassays, *Lab Chip*, 2015, **15**(18), 3776–3784.
31 A. H. C. Ng, M. D. Chamberlain, H. Situ, V. Lee and A. R. Wheeler, Digital microfluidic immunocytochemistry in single cells, *Nat. Commun.*, 2015, **6**(1), 7513.
32 R. Fobel, C. Fobel and A. R. Wheeler, DropBot: An open-source digital microfluidic control system with precise control of electrostatic driving force and instantaneous drop velocity measurement, *Appl. Phys. Lett.*, 2013, **102**(19), 193513.
33 W. Wang, Precise Droplet Dispensing in Digital Microfluidics with Dumbbell-Shaped Electrodes, *Micromachines*, 2022, **13**(3), 484.
34 J. Achilles, H. Harms and S. Müller, Analysis of living S. cerevisiae cell states—A three color approach, *Cytometry, Part A*, 2006, **69**(3), 173–177.
35 K. Choi, A. H. C. Ng, R. Fobel, D. A. Chang-Yen, L. E. Yarnell and E. L. Pearson, *et al.*, Automated Digital Microfluidic Platform for Magnetic-Particle-Based Immunoassays with Optimization by Design of Experiments, *Anal. Chem.*, 2013, **85**(20), 9638–9646.
36 J. Michl, K. C. Park and P. Swietach, Evidence-based guidelines for controlling pH in mammalian live-cell culture systems, *Commun. Biol.*, 2019, **2**(1), 144.
37 J. Lamanna, E. Y. Scott, H. S. Edwards, M. D. Chamberlain, M. D. M. Dryden and J. Peng, *et al.*, Digital microfluidic isolation of single cells for -Omics, *Nat. Commun.*, 2020, **11**(1), 5632.
38 D. Witters, N. Vergauwe, S. Vermeir, F. Ceyssens, S. Liekens and R. Puers, *et al.*, Biofunctionalization of electrowetting-on-dielectric digital microfluidic chips for miniaturized cell-based applications, *Lab Chip*, 2011, **11**(16), 2790.
39 S. Srigunapalan, I. A. Eydelnant, C. A. Simmons and A. R. Wheeler, A digital microfluidic platform for primary cell culture and analysis, *Lab Chip*, 2012, **12**(2), 369–375.
40 A. P. Aijian and R. L. Garrell, Digital Microfluidics for Automated Hanging Drop Cell Spheroid Culture, *SLAS Technol.*, 2015, **20**(3), 283–295.
41 J. Zhai, H. Li, A. H. H. Wong, C. Dong, S. Yi and Y. Jia, *et al.*, A digital microfluidic system with 3D microstructures for single-cell culture, *Microsyst. Nanoeng.*, 2020, **6**(1), 6.
42 L. K. Fiddes, V. N. Luk, S. H. Au, A. H. C. Ng, V. Luk and E. Kumacheva, *et al.*, Hydrogel discs for digital microfluidics, *Biomicrofluidics*, 2012, **6**(1), 014112.
43 S. M. George and H. Moon, Digital microfluidic three-dimensional cell culture and chemical screening platform using alginate hydrogels, *Biomicrofluidics*, 2015, **9**(2), 024116.
44 B. A. Nestor, E. Samiei, R. Samanipour, A. Gupta, A. Van Den Berg and M. Diaz De Leon Derby, *et al.*, Digital microfluidic platform for dielectrophoretic patterning of cells encapsulated in hydrogel droplets, *RSC Adv.*, 2016, **6**(62), 57409–57416.
45 B. F. Bender, A. P. Aijian and R. L. Garrell, Digital microfluidics for spheroid-based invasion assays, *Lab Chip*, 2016, **16**(8), 1505–1513.
46 H. Y. Huang, H. H. Shen, C. H. Tien, C. J. Li, S. K. Fan and C. H. Liu, *et al.*, Digital Microfluidic Dynamic Culture of Mammalian Embryos on an Electrowetting on Dielectric (EWOD) Chip, *PLoS One*, 2015, **10**(5), e0124196.
47 M. Y. Chiang, Y. W. Hsu, H. Y. Hsieh, S. Y. Chen and S. K. Fan, Constructing 3D heterogeneous hydrogels from electrically manipulated prepolymer droplets and crosslinked microgels, *Sci. Adv.*, 2016, **2**(10), e1600964.
48 I. Barbulovic-Nad, S. H. Au and A. R. Wheeler, A microfluidic platform for complete mammalian cell culture, *Lab Chip*, 2010, **10**(12), 1536.
49 K. Wu, X. He, J. Wang, T. Pan, R. He and F. Kong, *et al.*, Recent progress of microfluidic chips in immunoassay, *Front. Bioeng. Biotechnol.*, 2022, **10**, 1112327.
50 M. Ho, A. Au, R. Flick, T. V. Vuong, A. A. Sklavounos and I. Swyer, *et al.*, Antifouling Properties of Pluronic and Tetronic Surfactants in Digital Microfluidics, *ACS Appl. Mater. Interfaces*, 2023, **15**(5), 6326–6337.
51 S. Jarusintanakorn, C. Phechkrajang, P. Khongkaew, E. Mastrobattista and M. Yamabhai, Determination of Chinese hamster ovary (CHO) cell densities and antibody titers from small volumes of cell culture supernatants using multivariate analysis and partial least squares regression of UV-Vis spectra, *Anal. Bioanal. Chem.*, 2021, **413**(23), 5743–5753.
52 J. Schütt, B. Ibarlucea, R. Illing, F. Zörgiebel, S. Pregl and D. Nozaki, *et al.*, Compact Nanowire Sensors Probe Microdroplets, *Nano Lett.*, 2016, **16**(8), 4991–5000.
53 Y. Wang, L. Zhao, A. Xu, L. Wang, L. Zhang and S. Liu, *et al.*, Detecting enzymatic reactions in penicillinase via liquid crystal microdroplet-based pH sensor, *Sens. Actuators, B*, 2018, **258**, 1090–1098.
54 D. Welch and J. B. Christen, Real-time feedback control of pH within microfluidics using integrated sensing and actuation, *Lab Chip*, 2014, **14**(6), 1191.

55 M. Tovar, L. Mahler, S. Buchheim, M. Roth and M. A. Rosenbaum, Monitoring and external control of pH in microfluidic droplets during microbial culturing, *Microb. Cell Fact.*, 2020, **19**(1), 16.
56 H. Li, T. Peng, Y. Zhong, M. Liu, P. I. Mak and R. P. Martins, *et al.*, pH Regulator on Digital Microfluidics with Pico-Dosing Technique, *Biosensors*, 2023, **13**(11), 951.
57 X. Lin, W. Qiu, S. Bayer and S. Nagl, Optical pH Monitoring in Microdroplet Platforms for Live Cell Experiments Using Colloidal Surfactants, *Methods Mol. Biol.*, 2023, **2689**, 39–51.
58 J. Ehgartner, M. Strobl, J. M. Bolivar, D. Rabl, M. Rothbauer and P. Ertl, *et al.*, Simultaneous Determination of Oxygen and pH Inside Microfluidic Devices Using Core–Shell Nanosensors, *Anal. Chem.*, 2016, **88**(19), 9796–9804.
59 W. Qiu and S. Nagl, Automated Miniaturized Digital Microfluidic Antimicrobial Susceptibility Test Using a Chip-Integrated Optical Oxygen Sensor, *ACS Sens.*, 2021, **6**(3), 1147–1156.
60 S. A. Pfeiffer, S. M. Borisov and S. Nagl, In-line monitoring of pH and oxygen during enzymatic reactions in off-the-shelf all-glass microreactors using integrated luminescent microsensors, *Microchim. Acta*, 2017, **184**(2), 621–626.
61 K. Schmale, SENSOLUX® stand-alone version: noninvasive determination of pH and DO in shake flasks, *Nat. Methods*, 2009, **6**(11), iii–iv.
62 Z. Hetzler, Y. Wang, D. Krafft, S. Jamalzadegan, L. Overton and M. W. Kudenov, *et al.*, Flexible sensor patch for continuous carbon dioxide monitoring, *Front. Chem.*, 2022, **10**, 983523.
63 M. Tric, M. Lederle, L. Neuner, I. Dolgowjasow, P. Wiedemann and S. Wölfl, *et al.*, Optical biosensor optimized for continuous in-line glucose monitoring in animal cell culture, *Anal. Bioanal. Chem.*, 2017, **409**(24), 5711–5721.
64 Z. Tong, C. Shen, Q. Li, H. Yin and H. Mao, Combining sensors and actuators with electrowetting-on-dielectric (EWOD): advanced digital microfluidic systems for biomedical applications, *Analyst*, 2023, **148**(7), 1399–1421.
65 C. Dixon, A. H. C. Ng, R. Fobel, M. B. Miltenburg and A. R. Wheeler, An inkjet printed, roll-coated digital microfluidic device for inexpensive, miniaturized diagnostic assays, *Lab Chip*, 2016, **16**(23), 4560–4568.
66 K. Liu, Y. He, Z. Lu, Q. Xu, L. Wang and Z. Liu, *et al.*, Laser-induced graphene-based digital microfluidics (gDMF): a versatile platform with sub-one-dollar cost, *Lab Chip*, 2024, **24**(12), 3125–3134.
67 M. Abdelgawad and A. R. Wheeler, Low-cost, rapid-prototyping of digital microfluidics devices, *Microfluid. Nanofluid.*, 2008, **4**(4), 349–355.
68 M. Yafia, A. M. Foudeh, M. Tabrizian and H. Najjaran, Low-Cost Graphene-Based Digital Microfluidic System, *Micromachines*, 2020, **11**(9), 880.